A Stochastic Model for Crankshaft Transitions. II. Analysis of Transition Dynamics

Bruno Nigro and Giorgio J. Moro*

Dipartimento di Chimica Fisica, Università di Padova, via Loredan 2, 35131 Padova, Italy

Received: February 27, 2002; In Final Form: May 14, 2002

The three-rotor model introduced in part I (*J. Phys. Chem.* **1996**, *100*, 16419) displays transitions of crankshaft type between stable states that are not connected by saddle points of the potential. The method of site localizing functions is employed for characterizing the crankshaft process. We show that its rate is controlled by the torsional dynamics near the bifurcations of separatrices originating from the potential maximum. From the analysis of the probability flux, the picture of crankshaft transitions as sequential and concerted crossings of the barrier by two torsional angles is recovered, like in the concerted torsional transitions found in the simulations of polymers. The identification of the separatrix bifurcations leads to an analytical estimate of the crankshaft transition rate. Moreover, it is shown how such an estimate can be generalized to multidimensional stochastic problems, so opening the possibility of analyzing similar types of transitions from realistic models of torsional dynamics in polymers.

1. Introduction

As shown first by Kramers,[1] stochastic theories lead to a rather general description of kinetic processes in condensed phases on the basis of the energy profile for the relevant degrees of freedom and of the dissipation due to the thermal bath.[2] When the kinetic transition is controlled by the dynamics near the saddle point, analytical estimates of the rates are supplied by the Kramers−Langer theory,[3] which takes explicitly into account the coupling between reactive and nonreactive degrees of freedom. The analysis by Skolnick and Helfand[4,5] of conformational transitions of single bond type in polymers represents an important application of the Kramers−Langer theory. In this case the dynamical coupling between the different torsional angles has a primary role. Indeed, if the transition is represented as the independent rotation of one torsional angle only (the reactive degree of freedom), large swinging of the chain tails would result with a too-high friction opposing to the motion. Skolnick and Helfand have shown that the coupling with the other torsional angles (the nonreactive degrees of freedom) leads to a cooperative motion that reduces the tail swinging and therefore also the effective friction. Moreover, the application of the Kramers−Langer theory allows a detailed description of the dependence of single bond transitions on the conformational state of the chain.[4−6]

However, single bond transitions considered as independent kinetic processes are not sufficient to characterize exhaustively the conformational dynamics of polymers. Several molecular dynamics simulations of polymers have shown the occurrence of more complex processes usually described as correlated transitions of two torsional angles.[7−11] In this case a transition of a given bond seems to drive in short times a further transition on a next-to-nearest-neighbor bond. The interpretation and the modeling of these processes are still open issues since in the Kramers−Langer theory there is no room for correlation between crossings of different saddle points. It should be mentioned that Helfand has proposed a picture for them by invoking the chain stress due to a saddle point crossing, which favors the transition of a nearby torsional angle.[12] But such a point of view is still lacking of quantitative description.

On the other hand, an analogy exists with the so-called "crankshaft transitions," which many years ago where proposed on a purely phenomenological ground[13] as simultaneous rotations of two bonds (or even more, see the classification in refs14 and 15), avoiding large displacements of the tails. One might invoke such an interpretation for the correlated transitions of polymers, as long as in both cases at the end of the transition process the configurations of two torsional angles have been changed. But also such an interpretation lacks of a quantitative estimate of the transition rate. Moreover, the simple picture of crankshaft processes predicts the simultaneous transition of two torsional angles, while only a correlation on the time of their transition has been found in the simulations.

In the effort of providing a quantitative analysis of these processes, in ref 16 (hereafter denoted as part I), a simple stochastic model displaying transitions of crankshaft type was proposed. It can be depicted as three rotors constrained to rotate about a common axis (see Figure 1), with pairwise bistable potentials of interaction. Given the simple structure of the model, numerical solutions of the stochastic problem can be obtained, and from them one can derive the exact values of the rate coefficients of two independent kinetic processes. The former corresponds to standard single bond transitions, while the latter was assigned to transitions of crankshaft type since after the transition both the torsional angles have changed configuration as if the central rotor alone was rotated. It should be stressed out that the solution of the stochastic model allows the identification of crankshaft transitions on the basis of initial and final configurations of the system in a kinetic process, without assuming a particular transition dynamics. This leads to a generalized definition of crankshaft transitions since the simultaneous rotation of bonds invoked in the original proposal[13] is no longer required. The numerical results described in part I have shown that if the outer rotors have a friction coefficient large enough, then the rate coefficients for single-bond and crankshaft transitions tend to be comparable. This situation might correspond to that of polymer systems, with the outer

* Corresponding author.

10.1021/jp0205517 CCC: $22.00
Published on Web 06/20/2002

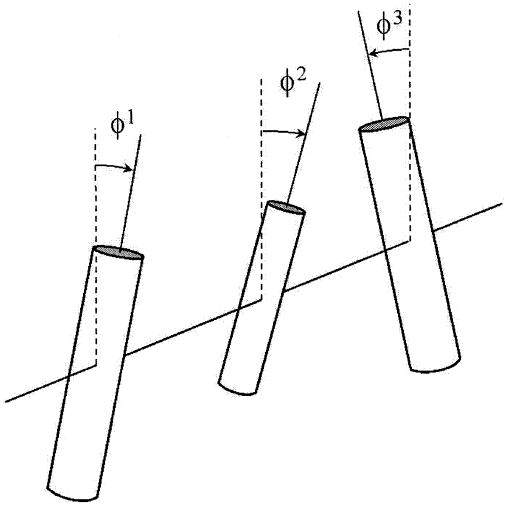

Figure 1. Model system represented as three rods rotating about a common axis.

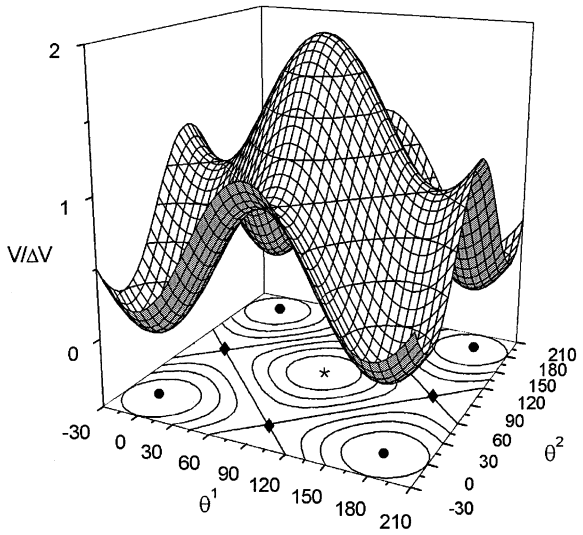

Figure 2. Profile of the internal potential equation (2.1) with the two-dimensional projection of equipotential lines separated by $\Delta V/4$ energy units. The minima (at $V = 0$), the saddle points (at $V/\Delta V = 1$), and the maxima (at $V/\Delta V = 2$) are denoted by circles, diamonds and stars, respectively.

rotor friction representative of the large friction opposing the rotations of the tails linked to the chain segment where a transition is localized.

To the best of our knowledge, part I is the only work that has demonstrated the existence of crankshaft transitions in a model system for a free chain. In the present work we intend to go beyond the numerical calculation of kinetic coefficients as reported in part I to gain a more detailed insight on the processes leading to crankshaft transitions. Our first objective is the characterization of the torsional angle dynamics during this type of processes, to establish whether any analogy exists with correlated transitions found in the simulations of polymers. A useful tool for the analysis of the stochastic dynamics leading to kinetic transitions is provided by the site-localizing functions,[17] which select the domain of the phase space pertinent to each stable state. Since they also provide an explicit relation for the transition rates, they can be used to characterize a specific kinetic process and its dependence on the features of the stochastic model (for instance the ratio between the rotor friction coefficients).

Our second main objective is the derivation of an estimate of asymptotic type for the rate of crankshaft transitions. It should be stressed out that the original Kramers−Langer theory cannot be applied to crankshaft transitions because of the absence of a saddle point crossing. The analysis of site-localizing functions, however, points out that also in this case there is a local control of the transition by a specific region of the torsional angle space. Thus the identification of this critical region, together with the generalization of the normal-mode analysis due to Langer,[3] leads to an analytical estimate for the rate of crankshaft transitions.

The paper is organized as follows. In the next section the three rotor model is illustrated together with the main results of part I. In the third section, the kinetic processes are analyzed by employing the site localizing functions that allow one to determine the stochastic separatrix and to characterize the probability flux during a transition. It will be shown that the main path for crankshaft processes corresponds to correlated transitions of the two torsional angles. In the following section, we will introduce the deterministic separatrix that allows a simple identification of the region of the torsional angle space which controls the crankshaft transitions. Then, by applying a normal-mode analysis, we shall derive an analytical estimate of crankshaft transitions that will be compared to the exact numerical results. In the fifth section, the asymptotic analysis of crankshaft transitions will be extended to systems described by multidimensional stochastic equation. In the final section, the main conclusions are presented together with an analysis of perspectives open by the new methodology proposed in the present work.

2. The Three-Rotor Model

Figure 1 provides the representation of the model as three rods with orientation angles (ϕ^1, ϕ^2, ϕ^3) and which are constrained to rotate about a common axis. We shall consider the system in the symmetric configuration, with the same friction coefficient ξ_o for the outer rods (ξ_i will denote the friction coefficient of the inner rod) and the same type of torsional potential for the two pairs of adjacent rods. By denoting with $\theta = (\theta^1, \theta^2) \equiv (\phi^2 - \phi^1, \phi^3 - \phi^2)$ the two torsional angles, the following internal potential with bistable torsional contributions having the minima at $\theta^j = 0, \pi$ will be employed:

$$V(\theta) = \frac{\Delta V}{2}[2 - \cos(2\theta^1) - \cos(2\theta^2)] \qquad (2.1)$$

where ΔV is the barrier height of each torsional potential. In Figure 2 the internal potential is represented together with some equipotential lines and the locations of minima, maxima, and saddle points. When dealing with conformational transitions, the overall rotational degree of freedom can be eliminated[18] by recovering the following Fokker−Planck−Smoluchowski equation[19,20] for the probability density $p(\theta, t)$ on the torsional angles

$$\partial p(\theta, t)/\partial t = -\Gamma(\theta)p(\theta, t)$$

$$\Gamma(\theta) = -\frac{\partial}{\partial\theta^j}D^{jk}p^{eq}(\theta)\frac{\partial}{\partial\theta^k}p^{eq}(\theta)^{-1}$$

$$D^{11} = D^{22} = k_B T/\xi_o + k_B T/\xi_i$$

$$D^{12} = D^{21} = -k_B T/\xi_i \qquad (2.2)$$

where $p^{eq}(\theta)$ denotes the equilibrium distribution

$$p^{eq}(\theta) = \frac{\exp\{-V(\theta)/k_B T\}}{Z}$$
$$Z = \int d\theta \exp\{-V(\theta)/k_B T\} \quad (2.3)$$

The convention of implicit summation of repeated indices will be used throughout the paper.

As the kinetic representation of the same system, one considers the time evolution of the populations $P_\alpha(t)$ for the four $\alpha = 1, 2, 3, 4$ independent stable states of the torsional angles corresponding to the four minima of the internal potential eq 2.1. These four stable states are represented in Figure 3 with the rods substituted by vertical lines with an arrow that allows one to recognize a rotation of a torsional angle. In the same figure we have also indicated all the possible transitions that can be partitioned into two classes: (i) the single bond transition with only one torsional angle changing between the two stable states and (ii) the crankshaft transitions when the starting and the final configurations differ by both the torsional angles. Because of the symmetric configuration of the system, the transitions within a class are characterized by the same rate constant, which will be denoted as w_s and w_c for the single bond and the crankshaft processes, respectively. The kinetic evolution equation can be written in all generality as

$$dP_\alpha(t)/dt = \sum_{\beta \neq \alpha} [P_\beta(t)\, w(\beta \rightarrow \alpha) - P_\alpha(t)\, w(\alpha \rightarrow \beta)] \quad (2.4)$$

where $w(\alpha \rightarrow \beta)$ denotes the rate constant for the transition from the state α to the state β and which can be identified with w_s or with w_c according to the type of transition.

The essential difference between the Fokker−Planck description (eq 2.2) and the kinetic description (eq 2.4) should be stressed. While the former describes in detail the stochastic evolution of the internal coordinates and it can be justified on the basis of statistical mechanics,[21] the latter describes only schematically the system without reference to the underlying degrees of freedom and it is normally accepted on a phenomenological basis. One of the main objectives of the Kramers theory[1] and its modern developments[2] is that of providing a clear connection between the kinetic description and the stochastic dynamics of the relevant degrees of freedom. Basically one invokes the time scale separation between the transition dynamics and the local relaxation within a potential well, both processes being described by the Fokker−Planck equation. Let us consider the eigenvalue problem for the evolution operator

$$\Gamma(\theta)\psi_n(\theta)p^{eq}(\theta) = \lambda_n \psi_n(\theta) p^{eq}(\theta) \quad (2.5)$$

with orthonormal eigenfunctions

$$\langle \psi_n |\, p^{eq} | \psi_m \rangle \equiv \int d\theta\, \psi_n(\theta) p^{eq}(\theta) \psi_m(\theta) = \delta_{n,m} \quad (2.6)$$

and the eigenvalues ordered in magnitude, $\lambda_0 < \lambda_1 \leq \lambda_2 \leq \cdots$, $\lambda_0 = 0$ being the vanishing eigenvalue for the stationary solution $\psi_0 = 1$. The eigenfunctions $\psi_n(\theta)$ represent the independent dynamical processes of the Fokker−Planck equation, with relaxation rates given by the corresponding eigenvalues λ_n. The generic time dependent probability can be decomposed as

$$p(\theta, t) = \sum_n c_n e^{-\lambda_n t} \psi_n(\theta) p^{eq}(\theta) \quad (2.7)$$

with the coefficients c_n determined by the initial distribution.[20] In the presence of high enough barriers, a large gap[22] is found between the first four eigenvalues, which describe the transition processes between stable states, and the remaining ones associated to the local relaxation within a potential well

$$\lambda_0, \lambda_1, \lambda_2, \lambda_3 \ll \lambda_4, \lambda_5, \cdots \quad (2.8)$$

Correspondingly a well-defined time scale separation between these two types of processes is recovered from the solution eq 2.2 of the Fokker−Planck equation. For the range of friction coefficients employed in Figure 4, a scaled barrier $\Delta V/k_B T = 5$ is sufficient to ensure a gap $\lambda_4/\lambda_3 \gtrsim 60$. Then the transition processes only are required to describe the long time behavior of the probability density eq 2.7, and the master equation 2.4 for the populations becomes an equivalent representation of the relaxation dynamics within such a time window. The formal equivalence of the two representations is conveniently derived by using the site-localizing functions[17] (see the next section), which allow one to specify a transition rate $w(\alpha \rightarrow \beta)$ according to the dynamical modes of the Fokker−Planck equation. In the case of our three-rotor model, one can follow a simpler and more direct procedure by exploiting the symmetries of the system that allow the analytical calculation of the independent relaxation rates of the master equation[16,23] from the two kinetic coefficients w_s and w_c. Then, by imposing the condition of equivalence between the relaxation rates of the master equation and the kinetic eigenvalues of the Fokker−Planck equation, one can specify the two elementary rates w_s and w_c according to the latter quantities. As long as the exact eigenvalues of the Fokker−Planck operator can be obtained numerically, such a procedure allows the determination of the rate coefficients without any approximation.

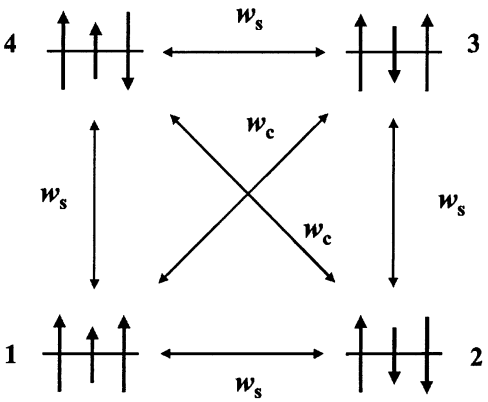

Figure 3. Kinetic scheme for the conformational transitions in the three-rotor model.

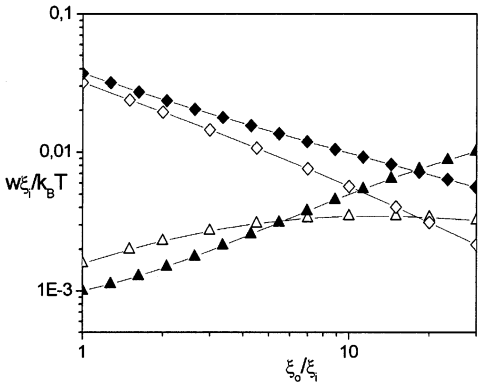

Figure 4. Friction dependence of the kinetic coefficients w_s (diamonds) for single bond transitions and w_c (triangles) for crankshaft transitions at $\Delta V/k_B T = 5$. Open symbols: exact values from the kinetic eigenvalues of the Fokker−Planck equation. Full symbols: analytical estimates (see section 4).

In Figure 4 these kinetic constants scaled by the diffusion coefficient of the inner rod (i.e., k_BT/ξ_i) are represented as functions of the friction ratio ξ_o/ξ_i for $\Delta V/k_BT = 5$ that, at room temperature, corresponds to the typical torsional barriers of alkyl chains. It should be emphasized that the model predicts that both single bond transitions and crankshaft transitions are always active. However, when the two friction coefficients are identical, the crankshaft transitions are slower by more than 1 order of magnitude with respect to single bond transitions. In this situation the crankshaft process is rather ineffective and it brings a negligible contribution to population relaxation of the conformers. On the other hand, by increasing the friction of the outer rods, the difference between the two kinetic coefficients decreases, and for $\xi_o/\xi_i \sim 10$ they become comparable. Correspondingly, the crankshaft transitions assume an important role in the conformational dynamics of the model system.

The friction dependence of the two rates can be understood on a qualitative basis. The single bond transitions always require the rotations of the outer rods. Then, for a given ξ_i, a rough inverse dependence of w_s with respect to ξ_o is expected. On the contrary, no rotation of the outer rods is invoked in the simple representation of crankshaft transitions as the rotation of the inner rod alone, so justifying the weak friction ξ_o dependence of w_c. This, however, is a too simplified picture of the effective crankshaft transitions, since it would predict the simultaneous overcoming of the two torsional barriers with twice the activation energy of the single bond transitions, that is a too-unfavorable energy factor[16] to be compensated by frictional effects in order to get comparable rates w_s and w_c. A more precise analysis is required in order to recover a realistic picture of crankshaft transitions.

3. Analysis of the Transition Dynamics

Let us introduce the site localizing function $G_\alpha(\theta)$ determining the population $P_\alpha(t)$ of conformer (or site, or stable state in a more general framework) α by integration with the probability density $p(\theta, t)$

$$P_\alpha(t) = \int d\theta\, G_\alpha(\theta) p(\theta, t) \tag{3.1}$$

As long as the population relaxation is driven by the kinetic processes of the Fokker−Planck operator without contamination by local relaxation processes, the site localizing functions should be specified as linear combination of the first four eigenfunctions $\psi_n(\theta)$. The coefficients of these linear combinations are derived from the condition that the site localizing function $G_\alpha(\theta)$ should select the phase space domain pertinent to the corresponding potential minimum θ_α. This can be achieved by imposing the constraints

$$G_\alpha(\theta_\beta) = \delta_{\alpha,\beta} \tag{3.2}$$

that is, that the site localizing function G_α must be unitary (vanish) at the corresponding potential minimum (at the other minima). One can show that eq 3.2 is sufficient to determine unambiguously the site localizing functions on the basis of kinetic eigenfunctions of the Fokker−Planck operator.[17] Moreover, from the time derivative of eq 3.1, the master equation 2.4 is recovered with the following definition of rate coefficients[17]:

$$w(\alpha \rightarrow \beta) = -\sum_\gamma (\mathbf{S}^{-1})_{\alpha,\gamma} \langle G_\gamma | \Gamma p^{eq} | G_\beta \rangle \tag{3.3}$$

where **S** is the superposition matrix of the site localizing functions

$$S_{\alpha,\beta} \equiv \langle G_\alpha |\, p^{eq} | G_\beta \rangle \tag{3.4}$$

For potential barriers large enough with respect to k_BT, there is a negligible superposition between different site localizing functions and the matrix **S** is nearly diagonal[17]

$$S_{\alpha,\beta} \simeq \delta_{\alpha,\beta} P_\alpha^{eq} \tag{3.5}$$

with, because of the symmetry, identical equilibrium populations $P_\alpha^{eq} = 1/4$ in the case of the three-rotor model. Then the relation for the transition rates can be simplified as

$$w(\alpha \rightarrow \beta) \simeq -\frac{1}{P_\alpha^{eq}} \langle G_\alpha | \Gamma p^{eq} | G_\beta \rangle$$

$$= -\frac{1}{P_\alpha^{eq}} \int d\theta\, p^{eq}(\theta)\, D^{jk} \frac{\partial G_\alpha(\theta)}{\partial \theta^j} \frac{\partial G_\beta(\theta)}{\partial \theta^k} \tag{3.6}$$

where an integration by parts has been performed in order to obtain the last equation. In this way it becomes evident that the transition rate between two states is determined by the corresponding pair of site localizing functions or, to be more precise, by their gradients weighted by the equilibrium distribution $p^{eq}(\theta)$.

The profile of the site localizing function $G_1(\theta)$ associated to the potential minimum at $\theta_1 = \theta_2 = 0$ is represented in Figure 5 in a particular case ($\Delta V/k_BT = 5$, $\xi_i = \xi_o$). Because of the symmetry of our model, the other site localizing functions are obtained by shifting $G_1(\theta)$ according to the location of the corresponding potential minima. As found in other two-dimensional problems,[17,24,25] the site localizing functions tend to a step function behavior, with the change from nearly unitary to vanishing values within a narrow strip about the so-called stochastic separatrix $\partial\Omega_\alpha$

$$\partial\Omega_\alpha: \quad G_\alpha(\theta) = 1/2 \tag{3.7}$$

The stochastic separatrix delimits the domain Ω_α pertinent to the stable state α, and it can be employed to characterize the main features of G_α from its shape in the bidimensional plot in the torsional angle space. In Figure 6, the stochastic separatrix for the site localizing functions $G_1(\theta)$ of Figure 5 is drawn together with the stochastic separatrices of the nearby states. In

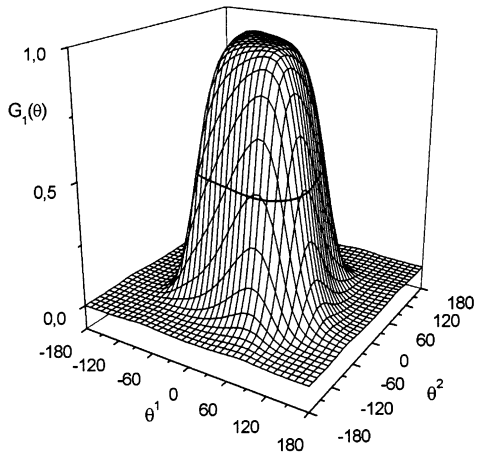

Figure 5. Profile of the site localizing function $G_1(\theta)$ for $\Delta V/k_BT = 5$ and $\xi_i = \xi_o$. The thick continuous line identifies the corresponding stochastic separatrix.

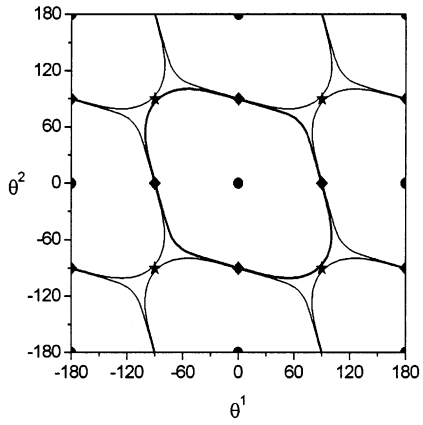

Figure 6. Stochastic separatrices for the site localizing function $G_1(\theta)$ (thick line) and for the nearby states (thin lines) with $\Delta V/k_BT = 5$ and $\xi_o = \xi_i$.

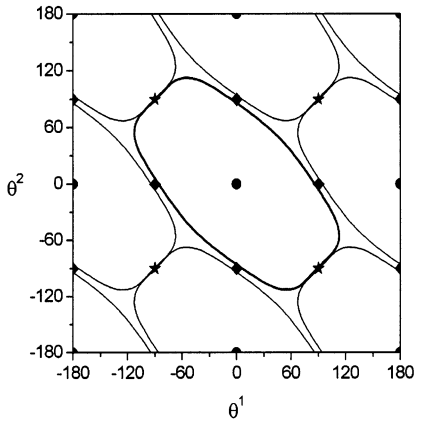

Figure 7. Stochastic separatrices for the site localizing function $G_1(\theta)$ (thick line) and for the nearby states (thin lines) with $\Delta V/k_BT = 5$ and $\xi_o = 10\xi_i$.

Figure 6, and in the following ones as well, the same symbols introduced in Figure 2 will be used to identify the potential minima, maxima, and saddle points. It should be noted that while the potential function has four-fold symmetry for rotations of the torsional angle plane about a minimum θ_α, the stochastic separatrix $\partial\Omega_\alpha$ (and the site localizing function G_α as well) has only a two-fold symmetry. As a matter of fact, the site localizing functions bear information of dynamical character and they must be consistent with the symmetry of the diffusion tensor, which is invariant with respect to π rotations only in the plane of torsional angles.

From the shape of the stochastic separatrices, information about the rate coefficients can be derived on the basis of eq 3.6. A nonvanishing gradient of a site localizing function, given its step-like behavior, is found only near the corresponding stochastic separatrix. Then, to recover a significant rate constant between two states, their stochastic separatrices should be in part nearly superimposed or close enough. This is the case for the separatrix $\partial\Omega_1$ and the separatrices of the other two states connected to the $\alpha = 1$ conformer by single bond transitions. They share a large portion of their separatrices in the region near the saddle point between two potential minima. Figure 6 allows also the comparison of $\partial\Omega_1$ with the separatrices of the states connected by crankshaft transitions. In these cases, one cannot find a clear superposition between the two separatrices, which tend to be adjacent only at the potential maximum. It should be evident that a small crankshaft transition rate is obtained from eq 3.6, when the same friction coefficient for the rotors is used as in Figure 6.

Let us now examine the effects of the increase of the friction ratio to $\xi_o/\xi_i = 10$ with the corresponding stochastic separatrices displayed in Figure 7. Now the separatrices of the conformers connected by a crankshaft transition are nearly superimposed in a well-defined interval centered at the potential maximum, so justifying the significant value of the corresponding rate.

To gain more insight on the local control of transition dynamics, one should examine the torsional angle dependence of the kernel whose integration leads to the rate coefficient eq 3.6, that is the function

$$p^{eq}(\theta)D^{jk}\frac{\partial G_\alpha(\theta)}{\partial\theta^j}\frac{\partial G_\beta(\theta)}{\partial\theta^k} \qquad (3.8)$$

A two-dimensional representation using a gray intensity scale is provided by Figure 8 for the single bond transitions, and by Figure 9 for the crankshaft transitions, both at $\xi_i/\xi_o = 10$. In

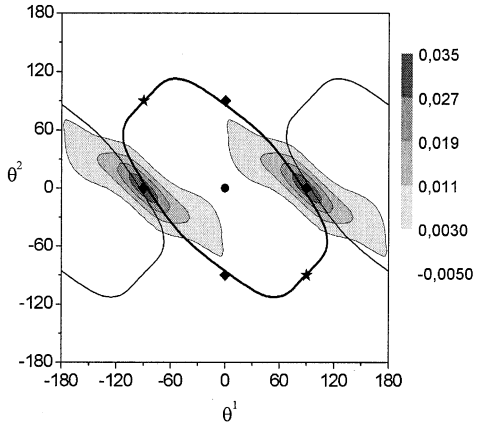

Figure 8. Torsional angle dependence of the kernel function eq 3.8 for a single bond transition in the same conditions of Figure 7.

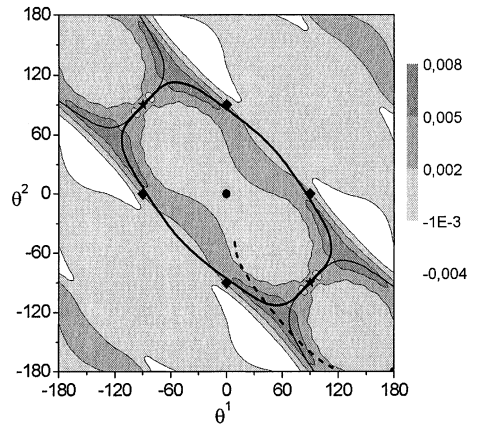

Figure 9. Torsional angle dependence of the kernel function eq 3.8 for the crankshaft transition in the same conditions of Figure 7. The dashed line represents a flow line through the region of separatrix bifurcation.

the former case a function with well-defined peaks centered at the saddle points is recovered. Therefore, the regions around the saddle points bring the largest contributions to the integral in eq 3.6 for the rate coefficient, in agreement with the Kramers−Langer[3] analysis that attributes to the saddle points a critical role in controlling the transition process. A function with a more complex behavior is found in the case of crankshaft transitions (Figure 9). Even in this case, however, one can identify the regions with the largest contributions to the rate coefficient, now in correspondence of the bifurcation of sepa-

ratrices leaving a potential maximum. This can be easily understood by taking into account that in the kernel eq 3.8 the gradients of site localizing functions are weighted by the equilibrium distribution $p^{eq}(\theta)$. Among the points with a nonvanishing product of the gradients of site localizing functions (i.e., the region where the two separatrices are adjacent), those with the largest weight $p^{eq}(\theta)$ are found near the separatrix bifurcation. For the sake of comparison, the potential maximum has comparable gradients of site localizing functions, but a significantly lower probability $p^{eq}(\theta)$. It should be mentioned that by applying the same kind of considerations to single bond transitions, one justifies the critical role of saddle points. Similarly, one can conclude that crankshaft transitions are controlled by the dynamics at points near the separatrix bifurcation. Thus crankshaft transitions cannot be visualized as the simultaneous rotation of two torsional angles, which would require the crossing of a potential maximum. Evidently in this process a more complex torsional dynamics is realized by avoiding the potential maximum in order to lower the energy barrier to be surmounted.[16]

To get a direct picture of torsional dynamics in a crankshaft transition, one can examine the flux determined by the site localizing functions. The Fokker−Planck equation 2.2 can be rewritten as conservation law of the probability

$$\frac{\partial}{\partial t}p(\theta, t) = -\frac{\partial}{\partial \theta^j} J^j(\theta, t) \tag{3.9}$$

with the following flux field

$$J^j(\theta, t) = -p^{eq}(\theta) D^{jk} \frac{\partial}{\partial \theta^k} p(\theta, t)/p^{eq}(\theta) \tag{3.10}$$

Let us suppose that initially the system is in a pure conformational state, for instance that only the conformer $\alpha = 1$ is populated

$$P_\alpha(0) = \delta_{\alpha,1} \tag{3.11}$$

The formal connection between conformer populations and probability density by means of site localizing functions allows us to reconstruct the probability distribution corresponding to eq 3.11

$$p(\theta, 0) = \sum_\beta (\boldsymbol{S}^{-1})_{1,\beta} G_\beta(\theta) p^{eq}(\theta) \simeq G_1(\theta) p^{eq}(\theta)/P_1^{eq} \tag{3.12}$$

The corresponding flux field

$$J^j(\theta, 0) \simeq -\frac{p^{eq}(\theta)}{P_1^{eq}} D^{jk} \frac{\partial G_1(\theta)}{\partial \theta^k} \tag{3.13}$$

describes the probability flow that, from the $\alpha = 1$ conformer, populates the other states. One could also examine the flux at later times, but this would be affected by the backward transitions and the transitions between the other conformers. The simpler characterization of the flux is provided by the flow lines that are locally tangent to the flux field,[25] and which describe the directionality of the torsional dynamics in the transitions. These flow lines begin inside the domain Ω_1 and end up in one of the nearby domains of the states connected by a transition.

To characterize the crankshaft dynamics, we have reported in Figure 9 also a typical flow line passing through the region of separatrix bifurcation. By identifying this flow line with a typical trajectory for a crankshaft transition, one can figure out the evolution of torsional angles during such a process. This leads to a picture of crankshaft process as a sequence of two torsional transitions in opposite direction at different times. Indeed, first θ^2 attains the value of $-\pi/2$, and only at a later time the transition at $\pi/2$ is detected for θ^1. To display more clearly such a behavior, we have plotted in Figure 10 the values of the two angles as a function of the length l along the flow line. If some monotonic relation is assumed between the time and the length l, then the behavior of Figure 10 can be interpreted as a sequence of two concerted single bond transitions. The delay between these events can be varied by examining nearby flow lines. The analogy with the concerted transitions found in the simulations of polymers[7−11] is striking, and it suggests that the stochastic treatment of crankshaft transitions might explain them.

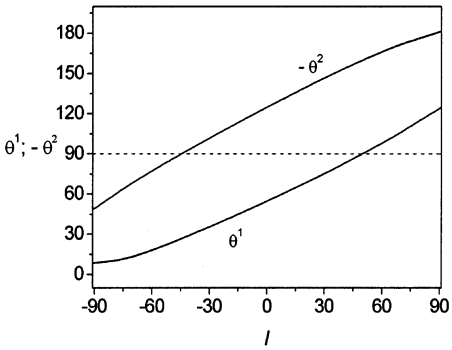

Figure 10. Torsional angle displacements along the flow line displayed in Figure 9.

It should be mentioned that by examining a flow line through the separatrix bifurcation in the opposite side of the same potential maximum, one would obtain an inverted sequence of torsional transitions (first θ^1 and then θ^2). There are two other separatrix bifurcations (see Figure 9) in correspondence of the opposite maximum, and they are associated to the crankshaft transition in the opposite direction (i.e., decrease of θ^1 and increment of θ^2).

4. Estimate of the Transition Rate

The availability of an analytical estimate of the transition rate is essential in order to complete the characterization of crankshaft processes. The previous analysis was relying on the exact solutions of the Fokker−Planck equation, which are not easily obtained in other model systems, in particular those having a large number of stochastic variables. Moreover, only an analytical form of the rate coefficient allows one to identify the features of a given system which control the crankshaft transitions. In the following we develop the methods for the analysis of two-dimensional models such as the three-rotor system, while in the next section the generalization to multidimensional problems will be presented.

From the previous section results, it should be evident that the separatrix is essential for the analysis of crankshaft processes. On the other hand, the stochastic separatrix requires the knowledge of the exact solutions of the Fokker−Planck operator for the calculation of the site localizing functions. Therefore, one must first derive an approximation to the true stochastic separatrix, and this is easily done by employing the following deterministic equation:

$$\frac{\mathrm{d}}{\mathrm{d}t}\theta^j(t) = -D^{jk}\frac{\partial V(\theta)/k_B T}{\partial \theta^k} \tag{4.1}$$

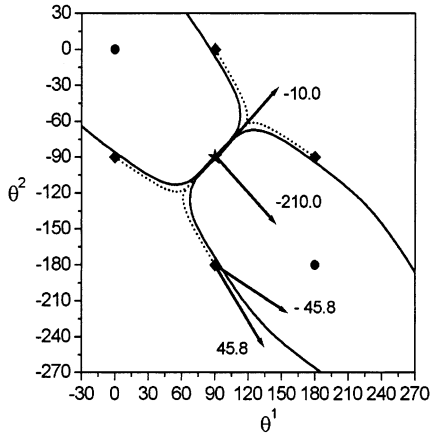

Figure 11. Deterministic (dotted lines) and stochastic (continuous lines) separatrices in the same conditions of Figure 7. The arrows denote the directions of the normal modes at the singular points.

which can be identified with the generalized Langevin equation associated to the Fokker−Planck equation 2.2 and devoid of the noise contribution.[20] The solutions of eq 4.1 can be represented as an ensemble of trajectories leaving the potential maxima and ending up in the potential minima. These trajectories cover all the torsional angle space (θ_1, θ_2), except for a point set of zero measure which includes the separate trajectories starting at the potential maxima but ending up at the saddle points. Then, on the basis of the fate of the deterministic trajectories, one can define a domain of attraction[26] $\hat{\Omega}_\alpha$ by including all the phase points belonging to trajectories ending up at the potential minimum θ_α. The boundaries of these domains are drawn by the trajectories that end up at a saddle point, and which determine the deterministic separatrix[26] $\partial\hat{\Omega}_\alpha$ of the attraction domain $\hat{\Omega}_\alpha$. These deterministic separatrices can be taken as approximations of the true stochastic separatrices,[17] albeit in particular systems there are systematic deviations[24] which, however, are absent in our model. The quality of the approximation can be appreciated from the comparison in Figure 11 of the stochastic and the deterministic separatrices in the same conditions of Figure 7. It should be mentioned that the deterministic trajectories, and therefore also the determinsitic separatrix, can be easily calculated numerically by substituting the time derivative in eq 4.1 with its finite difference approximation.

To characterize the dynamics near the singular points, we perform a normal-mode analysis in the same spirit of the Langer treatment of saddle point crossing.[3] By considering small displacements $\Delta\theta \equiv \theta - \theta_S$ from a singular point θ_S of the potential $V(\theta)$ (which could be either a maximum or a saddle point, or even a minimum), the deterministic eq 4.1 can be approximated as

$$\frac{\mathrm{d}}{\mathrm{d}t}\Delta\theta^j(t) = -D^{jk}V_{km}(S)\Delta\theta^m(t)/k_\mathrm{B}T \tag{4.2}$$

where $V_{km}(S)$ is the curvature matrix of the potential at the singular point θ_S

$$V_{jk}(S) \equiv \left(\frac{\partial^2 V(\theta)}{\partial\theta^j\partial\theta^k}\right)_{\theta=\theta_S} \tag{4.3}$$

Because of its linear structure, eq 4.2 can be solved through a normal-mode analysis according to the eigenvalue problem

$$D^{jk}V_{km}(S)s^m(n)/k_\mathrm{B}T = \omega(n)s^j(n) \tag{4.4}$$

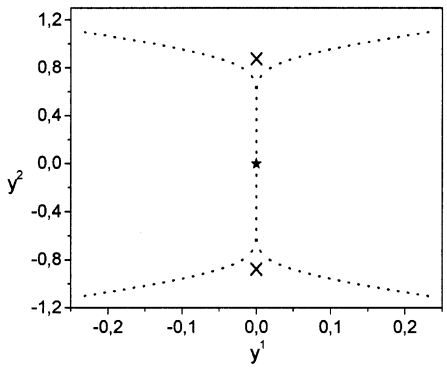

Figure 12. Deterministic separatrices represented in the plane of the normal modes.

where the vector $s^j(n)$ determines the direction in the torsional angle space of the nth normal mode having a frequency $\omega(n)$, in the following ordered as $\omega(1) < \omega(2)$. The normal mode directions for the saddle points and the potential maxima are represented in Figure 11 as arrows and they are labeled by the numerical value of the corresponding frequencies $\omega(n)$ scaled by $k_\mathrm{B}T/\xi_\mathrm{i}$. At the saddle point, the frequencies have opposite sign; the negative one corresponds to the reactive mode, while the nonreactive mode with positive frequency is parallel to the separatrices at the saddle point. A similar picture is recovered also for the potential maximum, with one normal mode parallel to the separatrices and the other in the direction of flow lines crossing the maximum. In this case, however, both frequencies are negative, and the reactive mode has the higher modulus frequency, i.e., $\omega(1)$. One should notice the large difference in magnitude between the two frequencies.

In the previous section we have shown that the region around the bifurcation of separatrices controls the crankshaft process. The analysis of the corresponding rate needs the characterization of such a region through the definition of a suitable bifurcation point in the torsional angle space. For this purpose it is convenient to represent the trajectories (the deterministic separatrix as well) as displacements along the normal modes by employing the coordinates $y = (y^1, y^2)$ defined as

$$y^n \equiv s_j(n)\Delta\theta^j \tag{4.5}$$

where $s_j(m)$ are the bi-orthogonal directions as specified in the Appendix. The deterministic equation 4.2 is then factorized with respect to these coordinates

$$\frac{\mathrm{d}}{\mathrm{d}t}y^n(t) = -\omega(n)y^n(t) \tag{4.6}$$

and the trajectories leaving the potential maximum can be parameterized as

$$\frac{|y^1(t)|^{1/\omega(1)}}{|y^2(t)|^{1/\omega(2)}} = \text{constant} \tag{4.7}$$

Because of the large frequency ratio $\omega(1)/\omega(2)$, these trajectories are highly distorted toward the y^2 axis. This effect becomes particularly evident in the trajectories representing the deterministic separatrices which are parameterized as

$$(y^1(\eta), y^2(\eta)) \tag{4.8}$$

where a η is a length parameter. In Figure 12 the deterministic separatrices are drawn in the (y^1, y^2) plane for the same case of the previous figure. The two separatrices nearly coincide for a

segment of the y^2 axis, and then bifurcate rather abruptly. The bifurcation points can be located along the y^2 axis, say at $y_p^2 \equiv y^2(\eta_p)$, where the label $p = \pm$ distinguishes the upper and the lower branch of the separatrices. A distance between the two separatrices must be selected in order to identify the bifurcation points. We use the condition that at y_p^2 the separatrix distance from the y^2 axis is half the width σ of the site localizing function (to be determined later on):

$$\eta_p: \quad y^1(\eta_p) = \sigma/2 \tag{4.9}$$

It should be emphasized that the locations y_p^2 are weakly dependent on the width parameter because the separatices bifurcate rather quickly. In Figure 12 the bifurcation points determined in this way are identified by crosses. Then, in evaluating the transition rate, we approximate the adjacent part of the deterministic separatrices by the segment of the y^2 axis between the two bifurcation points, that is the points

$$(0, y^2) \quad \text{for } y_-^2 \le y^2 \le y_+^2 \tag{4.10}$$

The shape of the site localizing functions near a singular point has now to be determined. For this purpose, we transform the Fokker−Planck equation 2.2 to the y representation (see the Appendix)

$$\partial p(y, t)/\partial t = -\Gamma(y)p(y, t)$$
$$\Gamma(y) = -\sum_n \frac{\partial}{\partial y^n}\exp\{-V(y)/k_BT\}\frac{\partial}{\partial y^n}\exp\{V(y)/k_BT\} \tag{4.11}$$

with independent contributions for the two normal modes. By employing local stationary solutions for approximating the site localizing functions[24,26]

$$\Gamma(y)p^{eq}(y)G_\alpha(y) = 0 \tag{4.12}$$

one derives a solution with an error function[27] dependence along the reactive mode

$$G_\alpha(y) = \frac{1}{2} \pm \frac{1}{2}\mathrm{erf}(y^1/\sigma) \tag{4.13}$$

the width being determined by the frequency of the same mode

$$1/\sigma = \sqrt{|\omega(1)|/2} \tag{4.14}$$

The sign + (−) should be used in eq 4.13 if the potential minimum θ_α corresponds to a positive (negative) coordinate y^1. Notice that eq 4.13, with an opposite sign, describes the other site localizing function G_β sharing the separatrix, so that $G_\beta(y^1) = 1 - G_\alpha(y^1)$. Moreover, the same functional form approximates also the site localizing functions near the saddle point (of course with a different value for σ). Thus, the approximation of eq 4.13 for the site localizing functions can be used for evaluating the rate of both crankshaft transitions and single bond transitions. One should employ eq 3.6 in the y representation

$$P_\alpha^{eq}w(\alpha \to \beta) = \sqrt{\det\{D^{ij}\}}\int \mathrm{d}y \frac{\exp\{-V(y)/k_BT\}}{Z}\left(\frac{\mathrm{d}G_\alpha(y^1)}{\mathrm{d}y^1}\right)^2$$
$$= \frac{\sqrt{\det\{D^{ij}\}}}{Z\pi\sigma^2}\int \mathrm{d}y \exp\{-|\omega(1)|(y^1)^2 - V(y)/k_BT\} \tag{4.15}$$

where the integration on y^2 has to be confined to the domain where the two separatrices $\partial\hat{\Omega}_\alpha$ and $\partial\hat{\Omega}_\beta$ are adjacent, while an infinite domain can be used for y^1.

Let us first examine how the single bond transition rate is obtained, by identifying the singular point θ_S with the saddle point. By substituting $V(y)$ with its quadratic expansion equation (A.7), and by extending to infinity the integration on y^2 because of the steep increase of the potential function along this coordinate, the following relation is obtained:

$$P_\alpha^{eq}w(\alpha \to \beta) = \frac{2}{Z\sigma^2}\sqrt{\det\{D^{ij}\}/|\prod_n \omega(n)|}\exp\{-V(S)/k_BT\}$$
$$= \frac{2}{Z\sigma^2}\frac{\exp\{-V(S)/k_BT\}}{\sqrt{|\det\{V_{ij}(S)/k_BT\}|}} \tag{4.16}$$

where eq A.5 has been employed to derive the last equation and $V(S) \equiv V(\theta_S)$. To recover the rate coefficient in a compact form, also the equilibrium population P_α^{eq} has to be specified according to the quadratic expansion eq A.6 with $\theta_S = \theta_\alpha$

$$P_\alpha^{eq} = \int \mathrm{d}\theta \frac{\exp\{-V(\alpha)/k_BT - V_{ij}(\alpha)\Delta\theta^i\Delta\theta^j/2k_BT\}}{Z} = \frac{\exp\{-F(\alpha)/k_BT\}}{Z} \tag{4.17}$$

where we have identified the free energy of the α state according to the relation[17,24]

$$F(\alpha) = V(\alpha) + \frac{k_BT}{2}\ln|\det\{V_{ij}(\alpha)/2\pi k_BT\}| \tag{4.18}$$

Then the rate coefficient for the transition crossing the saddle point S is written as

$$w(\alpha \to \beta) = \frac{|\omega(1)|}{2\pi}\exp\{-[F(S) - F(\alpha)]/k_BT\} \tag{4.19}$$

where the same definition eq 4.18 has been applied also for calculating the free energy $F(S)$ at the saddle point. The transition rate specified according to eq 4.19, which is equivalent to the Langer result[2] in the overdamped regime, is particularly appealing because of the identification of the frequency factor with the frequency $\omega(1)$ of the reactive mode. Notice that the rate w_s of single bond transitions in the three rotor model is twice eq 4.19, since the crossings of two equivalent saddle points contribute to the overall process.

A similar procedure can be applied also to crankshaft transitions, with eq 4.15 specified as

$$P_\alpha^{eq} w(\alpha \rightarrow \beta) = \frac{\det\{D^{ij}\}}{Z\pi\sigma^2} \exp\{-V(S)/k_B T\} \times \int_{-\infty}^{+\infty} dy^1 \int_{y_-^2}^{y_+^2} dy^2 \exp\{-|\omega(1)|(y^1)^2 - V(y)/k_B T\} \quad (4.20)$$

where the integration domain of y^2 has been limited to the common part of the deterministic separatrices according to eq 4.10. Then by inserting the quadratic expansion eq A.7 of the potential maximum, one obtains the following relation

$$w(\alpha \rightarrow \beta) = \frac{|\omega(1)|}{\sqrt{\det\{V_{ij}(S)/k_B T\}}} \sum_{p=\pm} \frac{f_D(|y_p^2|\sqrt{|\omega(2)|/2})}{\sqrt{\pi}} \times \exp\{F(\alpha)/k_B T - V(y_p)/k_B T\} \quad (4.21)$$

where f_D is the Dawson function[27]

$$f_D(x) \equiv e^{-x^2} \int_0^x dt\, e^{t^2} \quad (4.22)$$

and $y_p = (0, y_p^2)$ are the bifurcation points, which in the following are denoted also as S_p while S stands for the corresponding singular point of the potential, i.e., its maximum. By introducing the free energy of the activated state for crankshaft transitions in analogy to eq 4.18 with the potential function evaluated at the bifurcation points

$$F(S_p) = V(S_p) + \frac{k_B T}{2} \ln |\det\{V_{ij}(S)/2\pi k_B T\}| \quad (4.23)$$

the following relation for the rate coefficient is recovered

$$w(\alpha \rightarrow \beta) = \frac{|\omega(1)|}{2\pi} \sum_{p=\pm} \frac{f_D(\sqrt{\Delta V_p/k_B T})}{\sqrt{\pi}} \exp\{-[F(S_p) - F(\alpha)]/k_B T\} \quad (4.24)$$

where $\Delta V_p \equiv V(S) - V(S_p)$ is the difference of potential energy between the maximum and the bifurcation points. Besides the Dawson function factor $f_D/\sqrt{\pi}$ (with a value of 0.310 in the case of Figure 12), the relation for the rate of crankshaft transitions has the same structure of the standard approximation 4.19 for the rate of single bond transitions, with the saddle point free energy substituted by the free energy of the bifurcation points controlling the crankshaft process. It should be mentioned that the rate constant w_c for the three-rotor model is given by twice eq 4.24, since the rotations by π or by $-\pi$ of the inner rotor (which correspond to two different maxima of the torsional potential) lead to the same final configuration of the system.

Figure 4 allows the comparison between the exact values (open symbols) of both types of transitions and the previously described estimates (full symbols). It should be emphasized that, despite the approximations invoked in the derivation of eq 4.24, such an analytical relation provides the correct magnitude of the crankshaft transition rate and it accounts for its friction anisotropy dependence. Moreover, data shown in Figure 4 demonstrate that deviations from the exact values are comparable when examining single bond transitions on one hand, and crankshaft transitions on the other hand. This should not be unexpected since approximations eq 4.19 and eq 4.24 have been derived within a common framework provided by the site localizing functions. One can then conclude that the accuracy of the analytical approximation equation 4.24 for crankshaft transition rate is comparable to that of standard Kramers−Langer relations for saddle point crossings.

5. Generalization to Multidimensional Problems

The three-rotor model allows the study of a complex process like a crankshaft transition in a very simple system that, on one hand, can be solved exactly by using numerical methods[16] and that, on the other hand, facilitates the analytical treatment. However, real chain systems cannot be assimilated to the three-rotor model because of the absence of a common axis for the different torsional angles. Moreover, conformational dynamics of polymers require the description of dynamical effects of many torsional angles. Therefore, the results of the previous section should be generalized to multidimensional stochastic models in order to find application in the study of real chain systems.

Let us consider an N-dimensional stochastic problem described by the probability density $p(x, t)$ for the variables $x = (x^1, x^2, \cdots, x^N)$. For instance they can be identified with the ensemble of torsional angles describing a real polymer chain, or the torsional angles of a generalized $(N + 1)$ rotor model. Correspondingly, one can employ the following general form of the Fokker−Planck equation of Smoluchowski type

$$\partial p(x, t)/\partial t = -\Gamma(x) p(x, t)$$
$$\Gamma(x) = -(\partial/\partial x^j) D^{jk} p^{eq}(x) (\partial/\partial x^k) p^{eq}(x)^{-1} \quad (5.1)$$

The equilibrium distribution $p^{eq}(x)$ could be characterized on the basis of the internal mean field $V(x)$ as in eq 2.3.

The stable conformers of the systems can be identified from the minima x_α of $V(x)$, and for the corresponding conformer populations, a master equation like eq 2.4 can be assumed. In principle, if the kinetic eigenfunctions of $\Gamma(x)$ are known, also in this case one can derive the site localizing functions $G_\alpha(x)$ that generate the master equation (2.4), with eq 3.6 for the transition rate rewritten as

$$w(\alpha \rightarrow \beta) = \frac{1}{P_\alpha^{eq}} \int dx\, p^{eq}(x) D^{jk} \frac{\partial G_\alpha(x)}{\partial x^j} \frac{\partial G_\beta(x)}{\partial x^k} \quad (5.2)$$

As for the three-rotor model, the stochastic separatrix $\partial\Omega_\alpha$ that encloses the phase space domain Ω_α pertinent to the conformer α, is derived from the condition $G_\alpha(x) = 1/2$ on the corresponding site localizing function. Of course in this case the separatrix is represented by a surface in the N-th dimensional torsional space. The deterministic approximation for the separatrices can be derived from the analysis of the deterministic trajectories[24]

$$\frac{d}{dt} x^j(t) = -D^{jk} \frac{\partial V(x)/k_B T}{\partial x^k} \quad (5.3)$$

The saddle points, that is the singular points x_S of the potential, $\partial V(x)/\partial x^j|_{x=x_S} = 0$ with one negative principal curvature, represent the critical points for single bond transitions.[4−6] More complicated is the identification of the points controlling crankshaft transitions. Let us consider a simplified picture of such a process as the simultaneous crossing of two torsional angle barriers, the other torsional angles being fixed at their equilibrium configurations. This would correspond to a second-order singular point of the potential, the order of a singular point being identified with the number of negative principal curvatures. Of course a saddle point of second order is also a maximum for two-dimensional potentials such as in the three-

rotor model. To provide information about the corresponding site localizing function, the characterization of the deterministic separatrix is required in analogy to the treatment of the three-rotor model. Even if the calculation of a deterministic trajectory can be easily performed, the full sampling is not a simple task in the presence of an high dimensionality N of the space of torsional angles. A more direct procedure has to be employed. Let us consider the normal-mode analysis at a second-order singular point x_S associated to a crankshaft transition. The eigenvalue equation (4.4) for the normal modes is generalized as

$$D^{jk}V_{km}(S)s^m(n)/k_BT = \omega(n)s^j(n) \tag{5.4}$$

The first two normal modes have a negative frequency $\omega(n)$ and corresponds to deterministic trajectories leaving the singular points toward lower potential energies. The other normal modes with positive $\omega(n)$ describe the deterministic trajectories that from higher potential energies reach the singular point x_S. Therefore the deterministic trajectories leaving x_S have initially nonvanishing components

$$y^n = s_j(n)\Delta x^j \quad \Delta x^j \equiv x^j - x^j_S \tag{5.5}$$

only along the first two normal modes, $n = 1, 2$. Among them, there will be those ending up at a saddle point of first order, and they will be part of the deterministic separatrix. These elements of the deterministic separatrix can be easily determined since only a two-dimensional sampling in the (y^1, y^2) plane is required, and they can be represented in analogy to eq 4.8 as

$$(y^1(\eta), y^2(\eta), 0, 0, \cdots) \tag{5.6}$$

The characterization of their bifurcation can be done as for the three-rotor model, and the same type of approximation as eq 4.10 can be employed in the evaluation of the transition rate

$$(0, y^2, 0, 0, \cdots) \quad \text{for } y^2_- \le y^2 \le y^2_+ \tag{5.7}$$

The trajectories ending into x_S have null components along y^1 and y^2. They also belong to the deterministic separatrix which includes the singular point x_S. Therefore, further independent points of deterministic separatrix are

$$(0, 0, y^3, y^4, \cdots) \tag{5.8}$$

Since the normal mode components y^n evolve independently near the saddle point, one derives the following representation of the deterministic separatrix in agreement with eqs 5.7 and 5.8

$$(0, y^2, y^3, y^4, \cdots) \quad \text{for } y^2_- \le y^2 \le y^2_+ \tag{5.9}$$

It can be employed as an approximation of the shared part of the separatrices near x_S in the evaluation of the crankshaft transition rate.

Equation 4.15 is used for the evaluation of transition rates also in the multidimensional problem by integration on all the normal modes. The properties of the normal modes reported in the Appendix, like the quadratic expansion eq A.7 for the potential, are generalized to such a multidimensional problem by substituting $\Delta\theta^i$ with Δx^i. In particular, eq 4.18 is recovered for the single bond transitions controlled by saddle points. For the crankshaft transitions, the integration on the normal modes should be done according to eq 5.9. Therefore, eq 4.20 should be generalized by including integration on $y^3, y^4, \cdots$. However, because of the independent contribution of the normal modes to the expansion eq A.7 for the potential, eq 4.24 for the transition rate is again recovered and S_p is identified with $y_p = (0, y^2_p, 0, 0, \cdots)$. The multidimensional character is accounted for by the free energies eqs 4.18 and 4.23, with an explicit dependence on all the coefficients V_{ij} of the potential function expansion, and by the reactive normal-mode frequency $\omega(1)$, which depends on the dynamical coupling between all the coordinates x at the singular point.

6. Conclusions

The three rotor model has been analyzed in detail in order to characterize the crankshaft transitions. By describing the kinetic processes according to the site localizing functions,[17] it has been shown that these transitions are controlled by the flow near the bifurcation of separatrices. They correspond to sequential and correlated crossings by the two torsional angles of their potential barrier. Correspondingly, a lowering of the activation energy is achieved with respect to a simultaneous barrier crossing for the two torsional angles.[16] On the basis of the identification of the separatrix bifurcation, we have derived an analytical estimate for the crankshaft transition rate in the three-rotor model, which can be easily generalized to multidimensional stochastic models.

An analogy exists between the crankshaft transitions in the three rotor model and the correlated torsional transitions found in the simulations of polymers.[7−11] However, to verify the interpretation of the correlated torsional transitions according to the picture of transitions controlled by the separatrix bifurcation, an analysis of these stochastic processes in a realistic model for the torsional dynamics in polymers is required. Such an objective is now attainable thanks to the analytical estimate of transition rates which has been derived in the present work. We are currently developing the application of the theory to alkyl chains and to polymethylene.

Acknowledgment. The authors gratefully acknowledge financial support from MURST (PRIN ex 40%) and from EC (TMR contract FMRX CT97 0121).

Appendix: Properties of the Normal Modes

Let us consider the eigenvalue problem for the transposed matrix of eq 4.3

$$V_{km}(S)D^{mi}s_i(n)/k_BT = \omega(n)s_k(n) \tag{A.1}$$

The two sets of eigenvectors can be related as

$$s^m(n) = D^{mi}s_i(n) \tag{A.2}$$

and they can be made bi-orthonormal by properly choosing the normalization factors

$$s_m(n)s^m(n') = s_m(n)D^{mi}s_i(n') = \delta_{n,n'} \tag{A.3}$$

so that the definition eq 4.5 of normal mode coordinates can be inverted as

$$\Delta\theta^j = \sum_n s^j(n)y^n \tag{A.4}$$

Notice that the eigenvalue problem eq A.1 implies that

$$\det\{V_{km}(S)/k_BT\}\det\{D^{ij}\} = \prod_n \omega(n) \tag{A.5}$$

where $\det\{\cdots\}$ denotes the matrix determinant.

In proximity of the singular point θ_S, the potential function can be specified as

$$V(\theta) = V(S) + V_{ij}(S)\Delta\theta^i\Delta\theta^j/2 \tag{A.6}$$

where $V(S) \equiv V(\theta_S)$, or by transforming to the normal mode coordinates according to eq A.4

$$V(y) = V(S) + k_B T\sum_n \omega(n)(y^n)^2/2 \tag{A.7}$$

The integration element transforms into the normal mode coordinate representation as

$$d\theta = dy/\det\{\partial y^n/\partial\Delta\theta^j\} \tag{A.8}$$

with, according to eq 4.5,

$$\partial y^n/\partial\Delta\theta^j = s_j(n) \tag{A.9}$$

By using eq A.3 in order to specify the determinant, one obtains

$$d\theta = \sqrt{\det\{D^{ij}\}}dy \tag{A.10}$$

and this allows one to specify the probability density with respect to normal coordinates as

$$p(y, t) = \sqrt{\det\{D^{ij}\}}p(\theta, t) \tag{A.11}$$

By transforming the diffusion tensor[24]

$$\frac{\partial y^n}{\partial\Delta\theta^i}D^{ij}\frac{\partial y^{n'}}{\partial\Delta\theta^j} = s_i(n)D^{ij}s_j(n') = \delta_{n,n'} \tag{A.12}$$

the Fokker−Planck equation (4.11) in the y representation is easily derived.

References and Notes

(1) Kramers, H. A. *Physica* **1940**, *7*, 284.
(2) Hanggi, P.; Talkner P.; Borkovec, M. *Rev. Mod. Phys.* **1990**, *62*, 251.
(3) Langer, J. S. *Ann. Phys.* **1969**, *54*, 258.
(4) Skolnick, J.; Helfand, E. *J. Chem. Phys.* **1980**, *72*, 5489.
(5) Helfand, E.; Skolnick, J. *J. Chem. Phys.* **1982**, *77*, 5714.
(6) Ferrarini, A.; Moro, G.; Nordio, P. L. *Mol. Phys.* **1988**, *63*, 225. Moro, G. J.; Ferrarini, A.; Polimeno, A.; Nordio, P. L. In *Reactive and Flexible Molecules in Liquids*; Dorfmuller, Th., Ed.; Kluwer: Dordrecht, 1989; pp 107−139.
(7) Weber, T. A.; Helfand, E. *J. Phys. Chem.* **1983**, *87*, 2881.
(8) Ediger, M. D.; Adolf, D. B. *Adv. Polym. Sci.* **1994**, *116*, 73.
(9) Zuniga, I.; Bahar, I.; Dodge, R.; Mattice, W. L. *J. Chem. Phys.* **1991**, 5348.
(10) Boyd, R. H.; Gee, R. H.; Han, J.; Jin, Y. *J. Chem. Phys.* **1994**, *101*, 788.
(11) Brown, M. L.; Venable, R. M.; Pastor R. W. *Biopolymers* **1995**, *35*, 31.
(12) Helfand, E. *Science* **1984**, *226*, 647.
(13) Schatzki, T. F. *J. Polym. Sci.* **1962**, *57*, 496.
(14) Helfand, E. *J. Chem. Phys.* **1971**, *54*, 4651.
(15) Boyd, R. H.; Breitling, S. M. *Macromolecules* **1974**, *7*, 855.
(16) Moro, G. J. *J. Phys. Chem.* **1996**, *100*, 16419.
(17) Moro, G. J. *J. Chem. Phys.* **1995**, *103*, 7514.
(18) Moro, G. *Chem. Phys.* **1987**, *118*, 167, 181.
(19) van Kampen, N. G. *Stochastic Processes in Physics and Chemistry*; North-Holland: Amsterdam, 1992.
(20) Gardiner, C. W. *Handbook of Stochastic Methods*; Springer: Berlin, 1983.
(21) Hynes, J. T.; Deutch, J. M. In *Physical Chemistry. An Advanced Treatise*; Eyring, H., Henderson, D., Jost, W., Eds.; Academic Press: New York, 1975; Vol. XIB, p 729.
(22) Talkner, P. *Chem. Phys.* **1994**, *180*, 199.
(23) Ryter, D. *Physica* **1987**, *142A*, 103. Ryter, D.; Meyr, H. *Physica* **1987**, *142A*, 122.
(24) Moro, G. J.; Cardin, F. *Phys. Rev. E* **1997**, *55*, 4915.
(25) Moro, G. J.; Cardin, F. *Chem. Phys.* **1998**, *255*, 189.
(26) Schuss, Z. *Theory and Applications of Stochastic Differential Equations*; Wiley: New York, 1980.
(27) *Handbook of Mathematical Functions*; Abramowitz, W.; Stegun, I. A.; Eds.; Dover: New York, 1965.